Vokasi Unesa Bulletin of Engineering, Technology and Applied Science (VUBETA)
https://journal.unesa.ac.id/index.php/vubeta
Vol. 3, No. 3, 2026, pp. 481~502 DOI: 10.26740/vubeta.v3i3.49241
ISSN: 3064-0768

Topology Optimization of Passive UHF RFID Systems for Constrained Environments

Rahma Zayoud[1*], Habib Hamam[2]
[1,2]Faculty of Engineering, Université de Moncton, Moncton, NB E1A3E9, Canada
[2]School of Electrical Engineering, University of Johannesburg, Johannesburg 2006, South Africa
[2]International Institute of Technology and Management (IITG), Av. Grandes Ecoles, Libreville, Gabon
[2]Bridges for Academic Excellence - Spectrum, Tunis, Tunisia

Article Info

Article history:

Received December 17, 2025
Revised March 09, 2026
Accepted April 15, 2026

Keywords:

Passive Ultra-High Frequency
Radio Frequency Identification
Limitations
Accuracy
Physical topology configuration

ABSTRACT

Radio Frequency Identification (RFID), a remote identification and localization technology, utilizes electromagnetic and magnetic field properties and signal processing. However, this technology suffers from sensitivity issues such as liquids and metals, object movement, and collisions, which negatively affect its reading rate. To address this complex problem, we first demonstrate, based on theoretical principles, the strong relationship between the physical RFID topology configuration and its reading rate. Subsequently, we developed an application that determines the best possible reading rate in a hostile environment—where all RFID constraints are present—by optimizing the physical topology configuration. For this purpose, we used the simulated annealing algorithm as an optimization technique. The results are promising: the algorithm converged three times to the same optimal solution within a single run; it required 48.5% of total iterations to find this configuration, which achieved a reading rate of 42.5% in a hostile environment. This optimal rate is considered satisfactory, especially when compared to the initial configuration's reading rate of approximately 7.5% under the same conditions. Even across multiple runs in different environments, the algorithm shows good consistency.

1. INTRODUCTION

1.1 Background

Passive Ultra-High Frequency (UHF) Radio Frequency Identification (RFID) has become a cornerstone technology for contactless identification and tracking across logistics, healthcare, manufacturing, and retail applications. By leveraging electromagnetic coupling between readers and passive tags, RFID enables non-line-of-sight identification with low operational cost and extended reading ranges compared to optical or infrared solutions.

1.2 Problem

Despite these advantages, passive UHF RFID systems remain highly sensitive to environmental constraints. Liquids, metallic objects, dense tag populations, and object motion significantly degrade reading range, detection reliability, and system predictability. These limitations restrict large-scale deployment and often require costly, application-specific solutions. Addressing these challenges remains a central research problem in RFID system design.

1.3 Literature

Extensive research has examined the limitations of passive UHF RFID systems and proposed methods to mitigate performance degradation in constrained environments. Early studies focused on physical and material

*Corresponding Author
Email: author1@email.com

effects, such as the influence of metallic surfaces on read range and antenna behaviour [1], as well as the impact of liquids and object motion on signal attenuation and variability [2]-[4]. Alongside these empirical investigations, a complementary line of work formalized interrogation-zone modeling, aiming to estimate reading regions in real environments and to support practical coverage planning through simulation and analytical models [5], as well as interrogation-zone determination under multiplexed antenna configurations [9].

Parallel research efforts explored algorithmic, architectural, and protocol-level enhancements to improve reading rate, range, and accuracy [10]-[17]. This includes advances in multi-antenna systems, anti-collision techniques, signal processing, and adaptive reader configurations. Protocol-centric optimization remains an active area, where temporal analysis and tuning of anticollision mechanisms support higher reliability under dense-tag conditions [18].

A significant body of work has addressed localization and reader positioning, proposing fault-tolerant localization methods [19][20], spread-spectrum ranging techniques [21], bistatic and multi-view configurations [22][23], multiliterate techniques [24], Multi-Hypothesis Extended and a Multi-Hypothesis Unscented Kalman Filter (MHEKF and MHUKF) approaches [25], and multipath mitigation strategies [26][27]. In parallel, RFID network planning research frames deployment as an optimization problem—often multi-objective—where reader placement, directional antenna deployment, and k-coverage constraints are jointly optimized to reduce blind spots and increase coverage robustness [68][28].

A. Motroni et al. [29] and G. Martino et al. [30] validated experimental RFID tracking techniques, including SAR-based localization and beamforming. Further contributions focused on real-time evaluation tools and system-level improvements. P. Rossi et al. [31] assessed RFID localization based on backscatter signal analysis, while P. Brunet-Gil and S. López-Soriano [32] introduced a real-time evaluation of tag metrics, enabling pre-deployment assessment of system performance in specific environments. Researchers have also explored the optimization of RFID system components and positioning to mitigate environmental constraints [33].

Other studies have investigated motion-aware and dynamic RFID systems, analyzing the effect of tag velocity [34], conveyor-belt tracking [35], wireless pressure detection [36], phase-based localization [37][38], RFID polarization dependence [39], and electromagnetic coupling for motion estimation [40][41]. These contributions highlight that real deployments require stability under time-varying conditions, motivating not only better positioning strategies but also improved methods to measure performance consistently across scenarios.

Accordingly, an increasingly important stream of literature focuses on measurement, benchmarking, and standardized metrics for evaluating read performance. Benchmarking frameworks compare tags/readers under controlled and realistic supply-chain conditions, using KPIs such as read rate, read range, and accuracy, and emphasizing repeatability and laboratory-to-field transferability [42].

Multiple studies have proposed specialized antenna designs to address these material constraints. B. Muneer et al. [43] featured a meandered antenna for a wireless battery-free management system for next-generation electric vehicles. Gocen and Palandoken [44] analyzed dielectric background effects on tag performance. Ban and Kai [45] and R. A. Ramirez et al. [46] proposed a design maintaining consistent read range between on-metal and off-metal conditions, while S. Fu et al. [47] integrated RFID tags into an aluminum conductor. R. B. V. B. Simorangkir et al. [48] provided design guidelines for epidermal antennas optimized for body applications. In [49][50], the authors exploit Self-tuning RFID microchips to minimize communication degradation. And in [51], authors propose a novel design that incorporates six Planar Inverted-L Antennas (PILAs) to miniaturize Ultra-High Frequency Radio Frequency Identification (UHF-RFID) tags for tag efficiency enhancement when mounted on various conductive surfaces. M. A. Alsultan et al. [52] delve into the use of ultrahigh-frequency (UHF) radio-frequency identification (RFID) antennas as hydration sensors across various fabrics and frequency bands. Moreover, for metal-mountable applications, many specialized tag antenna designs were proposed; S. -R. Lee et al. [53] proposed a loop-coupled small antenna with enhanced bandwidth, M. Murugesh et al. [54] proposed a compact dipolar patch antenna using an interdigital capacitor, M. Murugesh and M. F. Akbar [55] developed a compact capacitively coupled meandered-slot serrated patch tag antenna.

Research also seeks to enhance robustness in metallic and harsh environments. Zhang et al. [56] improved antenna performance across air and metal mounting conditions, and C. Wu et al. [57] explored RFID sensors for infrastructure monitoring under metallic interference. Athauda et al. [58] developed a low-cost smart cart system, and Grosinger et al. [59] examined passive RFID resilience in radiation-heavy environments. Further novel applications include real-time liquid-level monitoring [60]-[62], on-metal tag designs [63][64], and in-motion tag identification systems [65].

To address robustness without constant manual intervention, recent work also explores system calibration and parameter tuning, including calibration-free approaches and nonlinear calibration methods for RFIDrelated sensing and operation stability [66], as well as power-independent or optimization-driven antenna/system strategies [67].

1.4 Research Gap

In real-world deployments, RFID performance is governed not only by protocol design or tag sensitivity but also by the physical topology configuration of the system—namely antenna positions, orientations, heights, and spatial relationships with tagged objects. Variations in topology directly influence electromagnetic propagation, polarization mismatch, multipath interference, and ultimately the shape and stability of the interrogation zone (IZ), which must often be modeled and planned under real constraints (obstructions, interference, and orientation variability) [68].

Most existing RFID deployments still rely on manual trial-and-error to adjust antenna placement. Users frequently test multiple tags, reader settings, and antenna configurations without a systematic optimization strategy, which is time-consuming and often fails to produce robust read performance in hostile environments involving metal, liquid, or motion. Although RFID components are standardized at the hardware level, there is still no widely adopted, user-facing solution that enables automatic, environment-aware optimization of physical topology together with repeatable performance assessment and parameter calibration (e.g., transmit power, sensitivity thresholds, dwell time, and antenna orientation policies) [66][67].

In a broader sense, this need aligns with the principle that effective intelligent systems should be evaluated and designed around contextual adaptation, interpretability, and trustworthiness, where systems that adapt to their environment and remain socially meaningful are emphasized as the most promising [69]. Despite significant progress, existing RFID solutions exhibit several critical limitations:

- G1- Hardware-Centric Optimization: Most approaches rely on specialized antennas, tags, or readers designed for specific materials or applications, limiting scalability and adaptability.
- G2- Lack of Topology-Aware Automation: Current systems do not provide automated tools to optimize physical topology configuration based on environmental conditions and performance feedback.
- G3- Application-Specific Solutions: Many proposed methods are validated only in narrowly defined scenarios and cannot be generalized across diverse deployment environments.
- G4- Manual Trial-and-Error Deployment: Practitioners are forced to rely on empirical testing without systematic guidance, often failing to reach optimal interrogation zone configurations.

As highlighted by prior work on interrogation zone optimization [70], the absence of a generic, adaptive topology-driven solution remains a fundamental unresolved challenge. This gap motivates the development of a self-configuring passive UHF RFID system capable of optimizing physical topology dynamically using algorithmic search rather than hardware specialization.

1.5 Solution

To address the sensitivity problem of passive UHF RFID systems and to correct all the gaps mentioned above that stand as obstacles to further development and wider use of this technology, we introduce a generic, adaptive identification framework based on physical topology optimization rather than hardware specialization. A physical topology configuration is the physical arrangement of the network's hardware components. The most optimized configuration is the physical topology that has the highest reading rate. Our solution consists of two parts: software and hardware. The software is an application developed by me where the optimization algorithm is installed. The Hardware part is an automated tripod-based system assisted by wheels and guided by the software to support dynamic antenna repositioning based on the algorithm output, facilitating deployment in real-world scenarios to address the practical challenges associated with manual configuration.

1.6 Novelties

The main contributions of this study are:

- C1- Topology–Performance Relationship: We formally demonstrate the strong relationship between RFID physical topology configuration and reading rate, grounded in electromagnetic propagation principles and experimental validation.
- C2- Generic Optimization Framework: We propose a universal passive UHF RFID identification system capable of adapting to diverse environmental constraints by optimizing antenna topology, without requiring specialized tags or readers.
- C3- Algorithm-Driven Topology Optimization: We develop a middleware solution implementing the simulated annealing algorithm to autonomously explore and converge toward optimal antenna configurations under real-world constraints.
- C4- Experimental Validation in Hostile Environments: The proposed system is validated in a realistic environment involving metallic objects, liquids, and motion, achieving a reading rate improvement from

approximately 7.5% to 42.5%, with repeated convergence to the same optimal configuration within a single run.

1.7 Paper structure

This article follows the IMRAD academic writing style and is organized into four sections as follows: Section 1 is the introduction, and it includes a clear background; a clear definition of the problem; the pertinent literature on the topic; the suggested solution; and the novelties. Section 2 is Comprehensive Theoretical Basics and Proposed Method. This section explores the theoretical foundations of passive UHF RFID sensitivity, focusing on electromagnetic propagation, material interaction, and the impact of motion, and describes the materials and methods, including the design of the middleware system, the optimization algorithm, and the experimental setup used for performance evaluation. Section 3 is Results and Discussion, and it presents and discusses the results of the optimization process, comparing the performance of simulated annealing with other algorithms under constrained conditions. Section 4 is the conclusion, and it concludes the study by summarizing the findings and outlining directions for future research.

2. COMPREHENSIVE THEORETICAL BASIC, USED MATERIALS AND PROPOSED METHOD

2.1. Theoretical Basic

This section explains the physical and mathematical foundations that justify the need for topology optimization in passive UHF RFID systems. It is organized into three subsections: electromagnetic coupling principles, material and propagation effects, and the impact of motion on RFID signal quality.

2.1.1. Electromagnetic Coupling in Passive UHF RFID Systems

RFID technology uses radio waves to identify objects on which an RFID tag is placed. The antenna of an RFID reader and the antenna of an RFID tag interact in two modes: inductive or magnetic coupling and radiative or electromagnetic coupling. UHF frequencies use electromagnetic coupling. In the far field, at a distance from the source approximately greater than the wavelength, the beam diverges to give rise to a spherical wave, locally planar. Passive UHF RFID tags extract their power from the electromagnetic waves emitted by the reader's antenna to use this energy to activate and respond to it.

The effects of electromagnetic propagation are crucial for these passive UHF RFID systems since these RFID tags contain no batteries and depend on the electromagnetic field for power and communication. The propagation effects encountered in commercial RFID systems can all be explained and predicted from the fundamentals of electromagnetic propagation.

The total loss of an RFID system's propagation path, as shown in Figure 1, contains several factors: loss of reflection due to the power reflected at the media-air boundaries, loss of attenuation in the medium with loss, and loss of spreading, which is simply due to the properties of antenna radiation. Each of these factors can be understood and predicted based on the properties of the material and the boundary conditions.

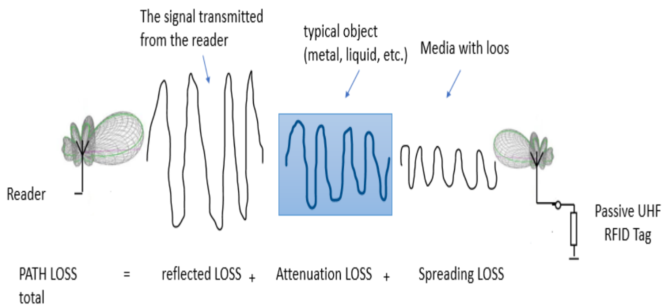

Figure 1. Basic propagation effects of an UHF RFID system

Using the harmonic temporal representation of electromagnetic fields and the well-known wave equation for fields in lossy media [71][72], it is possible to derive the propagation parameters in terms of material properties:

$$\nabla^2 E = j\omega\mu\sigma E - \omega^2\mu\varepsilon E \quad (1)$$

$$\nabla^2 H = j\omega\mu\sigma H - \omega^2\mu\varepsilon H \quad (2)$$

where $E, H \propto e^{j(k \cdot r - wt)}$

2.1.2. Material Properties and Propagation Losses

Since most commercial products are not pure conductors or pure dielectrics, it is convenient to create a relationship between complex permittivity and effective conductivity:

$$\varepsilon = \varepsilon' - j\varepsilon^{n} \quad (3)$$

$$\tan\delta \equiv \frac{\varepsilon''}{\varepsilon'} = \frac{\sigma}{\omega\varepsilon'}, \quad (4)$$

Given these material properties, it is then possible to define the complex propagation constant:

$$k = \omega\sqrt{\mu(\varepsilon' - j\varepsilon^{n})} \quad (5)$$

$$jk = \alpha + \beta = j\omega\sqrt{\mu\varepsilon\left[1 - j\left(\frac{\varepsilon'}{\varepsilon''}\right)\right]} \quad (6)$$

The propagation loss inside the material in Nepers per meter (or converted to dB per meter) is easily calculated from the imaginary part of the propagation constant:

$$\alpha = \omega\sqrt{\left(\frac{\mu\varepsilon'}{2}\right)\left[1 + \left(\frac{\varepsilon'}{\varepsilon''}\right)^{2} - 1\right]} \quad (7)$$

If we consider an arbitrarily marked object, then the loss of power due to reflections can be calculated by modeling it as a three-layer system (air-media-air) using the following reflection and transmission coefficients:

$$R = \frac{(1-Z_{12})(1+Z_{23})+(1+Z_{12})(1-Z_{23})e^{-2\gamma_2 d}}{(1+Z_{12})(1+Z_{23})+(1-Z_{12})(1-Z_{23})e^{-2\gamma_2 d}} \quad (8)$$

$$T = \frac{4}{(1-Z_{12})(1-Z_{23})e^{-\gamma_2 d}+(1+Z_{12})(1+Z_{23})e^{\gamma_2 d}} \quad (9)$$

where $Z_{ij} = \frac{\mu_i\gamma_j}{\mu_j\gamma_I}, i, j = 1, 2, 3 \ldots$

and $\gamma k = \pm\sqrt{j\omega\mu k(\sigma k + j\omega\varepsilon k)}$

Each Z_{ij} represents the impedance of air-medium-air materials. All the above theoretical explanations show the effect of metals or liquids on passive UHF RFID technology. Now, we proceed to analyze the effect of speed on RFID technology. For a passive UHF RFID tag that moves at speed v, as shown in Figure 2 [73], where:

$$d_2 + vt = d_1 \quad (10)$$

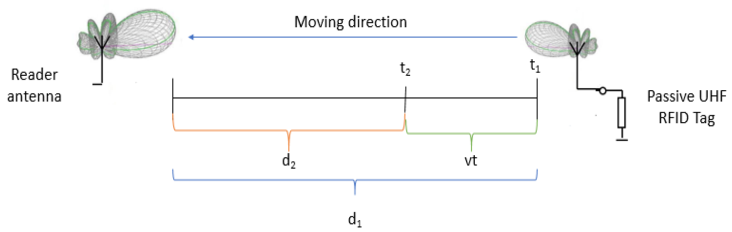

Figure 2. Example of a passive UHF RFID tag in motion

Based on the EPC Class-1 Generation-2 RFID protocol, the reader receives information from a passive tag by transmitting an unmodulated RF carrier and listening for a backscattered response. When the tag is moving at a constant speed, the carrier that the reader receives is different from the local carrier in frequency and initial phase due to the Doppler effect and the change in distance. These differences cause a change in the energy distribution between the IQ signals received over time.

The Doppler effect is the change in frequency or wavelength of a wave for an observer who moves relative to the wave source. The frequency difference caused by the Doppler effect differs between the transmission and reception links.

For the transmission link, where the reader (the source wave) is stationary while the tag (the observer) moves towards the reader, the frequency received by the tag is:

$$f_t = \left(1 + \frac{v}{c}\right)f_c \quad (11)$$

Where f_c is the carrier frequency transmitted by the reader, v is the speed of the moving tag, and c is the speed of the electromagnetic wave.

Meanwhile, for the reception link, where the tag (the observer) moves towards the stationary reader (the source wave), the carrier frequency received by the reader f_r is:

$$f_r = \frac{c}{c-v} f_t = \frac{c+v}{c-v} f_c \tag{12}$$

The change in distance causes the phase difference between the carrier that the reader receives and the initial carrier. The transmit and receive links contribute to the phase difference. We note the phase difference caused by the transmitting link by φ_t and the phase difference caused by the receiving link by φ_r. Thereafter, the total phase difference φ between the carrier received by the reader and the initial carrier is:

$$\varphi = \varphi_t + \varphi_r \tag{13}$$

For the transmission link, the carrier frequency is f_c for the reader. Consequently, the phase difference caused by the transmitting link φ_t is approximately:

$$\varphi_t = \frac{d}{\lambda} \times 2\pi = \frac{2\pi f_c d}{c} \tag{14}$$

Where d is the distance between the reader and the tag. We note the distance between the reader and the tag at t = 0 as d_0. Therefore, d satisfies:

$$d = d_0 - vt \tag{15}$$

For the reception link, the carrier frequency is f_r for the reader. Thus, the phase difference φ_r is:

$$\varphi_r = \frac{d}{\lambda} * 2\pi = \frac{2\pi f_c d}{c} * \frac{c+v}{c-v} \tag{16}$$

Connect (14) and (16) to (13) to obtain the total phase difference φ:

$$\varphi = \varphi_t + \varphi_r = 2\pi f_c d * \frac{2}{c-v} \tag{17}$$

Suppose that the initial carrier is sin $(2\pi f_c t)$. The final carrier received by the reader will be (18) when the frequency difference in (12) and the phase difference in (17) are considered.

$$\begin{aligned}\sin(2\pi f_r t - \varphi + \varphi_0) &= \sin\left(2\pi f_c t \frac{c+v}{c-v} - 2\pi f_c d * \frac{2}{c-v} + \varphi_0\right) \\ &= \sin\left(2\pi f_c t \frac{c+v}{c-v} - 2\pi f_c (d_0 - vt) * \frac{2}{c-v} + \varphi_0\right) \\ &= \sin\left[2\pi f_c t \left(1 + \frac{4v}{c-v}\right) - \frac{4\pi f_c d_0}{c-v} + \varphi_0\right]\end{aligned} \tag{18}$$

Where φ_0 is the constant of the phase difference caused by reflection.

We suppose that the initial oscillator I is:

$$\sin(2\pi f_c t) \tag{19}$$

and the initial oscillator Q is:

$$\cos(2\pi f_c t) \tag{20}$$

After mixing the backscattered carrier and filtering the frequency above f_c, the downlink mixed signals I and Q are:

$$I : \sin\left(2\pi f_c t \frac{4v}{c-v} - \frac{4\pi f_c d_0}{c-v} + \varphi_0\right) \tag{21}$$

$$Q : \cos\left(2\pi f_c t \frac{4v}{c-v} - \frac{4\pi f_c d_0}{c-v} + \varphi_0\right) \tag{22}$$

According to (21) (22), the total phase φ is:

$$\varphi = 2\pi f_c t \frac{4v}{c-v} - \frac{4\pi f_c d_0}{c-v} + \varphi_0 \tag{23}$$

φ determines the energy distribution and the initial phases of the baseband signal I and Q.

$$v_{pp-i} = \left|\sin\left(2\pi f_c t \frac{4v}{c-v} - \frac{4\pi f_c d_0}{c-v} + \varphi_0\right)\right| \tag{24}$$

$$v_{pp-q} = \left|\cos\left(2\pi f_c t \frac{4v}{c-v} - \frac{4\pi f_c d_0}{c-v} + \varphi_0\right)\right| \tag{25}$$

$$phase_i = sign\left[\sin\left(2\pi f_c t \frac{4v}{c-v} - \frac{4\pi f_c d_0}{c-v} + \varphi_0\right)\right] \tag{26}$$

$$phase_q = sign\left[\cos\left(2\pi f_c t \frac{4v}{c-v} - \frac{4\pi f_c d_0}{c-v} + \varphi_0\right)\right] \tag{27}$$

(24) - (27) show that when the tag moves at a constant speed towards the reader, the peak-to-peak values and the initial phases of the baseband signal I and Q change over time.

It is clear from the above that, theoretically, metals and liquids influence the reading range of the UHF RFID antenna, and that movement influences the antenna detection angle. So, bringing the antenna and the tag closer and changing the antenna orientation fixes those sensitivity problems. It is simple with a single UHF RFID antenna and a passive UHF RFID tag. Nevertheless, the task will be complicated with multiple antennas and several tags. In such a case, an optimization algorithm is necessary.

2.2. Passive UHF RFID Used Materials

The Passive UHF RFID materials that we used in our solution are the ALR-9900 Alien reader, 4 ALR-8696-C antennas and Passive UHF RFID Labels. The ALR-900 reader allows the user to connect 4 antennas. The antennas were chosen for their high performance and circular polarization, so they are stable and can detect more tags. The labels are the most popular type of UHF RFID tag, disposable, low-cost, and with a good reading range, averaging around 20 feet.

2.2. Proposed Method

Our proposed solution aims to optimize the physical topology of a passive UHF RFID identification system to make it suitable for applications with various constraints. It requires the development of software to calculate the optimal reading rate and the design of hardware to hold the RFID antennas that would be used in this system.

2.3.1 Hardware

The hardware part of the solution is 4 mechanical tripod systems. Each antenna will be installed on a bracket fixed on the tripod. The tripod system changes the distance between the antenna and the tag. The bracket changes the area, or the zone, covered by the antenna. Based on a well-known optimization algorithm integrated into the software of the solution, the antenna's location and its covered zone will be changed continuously till the optimal reading rate is found. The tripod system is supported by 3 wheels driven by the software to make the whole solution fully autonomous.

The brackets are each attached to a tripod system by a servo motor, as shown in Figure 3. These servomotors are controlled by the middleware to vary the angles of the detection connections in an automated manner to find the optimal topology. They will be connected to the computer, where the middleware is installed, by coaxial cables for their power. Mechanical tripod systems are removable supports allowing the software to control the antenna's coordination and tilting angle. After finding the optimal solution and installing the antennas according to the best possible physical topology, the user removes the supports. The various positions, heights, and inclinations of the four antennas used are generated and randomly selected by the middleware.

Figure 3. The mechanical design of the tripod system

We used four manipulator arms. One for each antenna. Each manipulator arm has 3 degrees of freedom of rotation, belongs to class 1, and can be oriented in all directions to correctly position the antenna using three servos. Each actuator manages a seal, as shown in Figure 4. The servomotors are controlled by an Arduino Uno card and a Bluetooth HC06 shield, which can communicate over a range of 10 meters. The computer (or server) communicates with the Arduino Uno card via Bluetooth communication to control the servomotors.

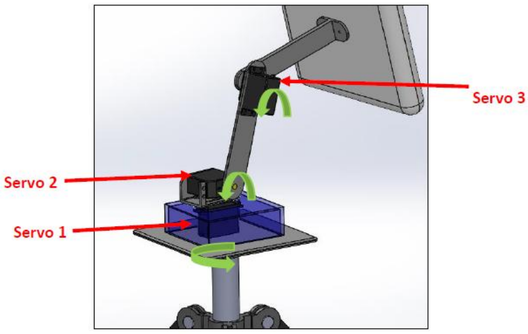

Figure 4. The mechanical structure of the manipulator arm

2.3.2 Software

The server is a Java application where the simulated annealing algorithm is implemented via the integrated development environment NetBeans. So, we manage those 4 manipulator arms to optimize the physical topology based on the implemented optimization algorithm's directives. We opted for the use of the simulated annealing algorithm because of its ability to overcome local maxima/minima. The server is also used for communication with the RFID reader through an RS232 serial connection and an Ethernet connection.

2.3.2.1 Solution's operation

Our solution involves the user entering the initial parameters into the application. The initial parameters are the number of tags in the environment, the length and the width of the environment, the number of expected configurations, and the number of UHF RFID antennas used. The more accurate this information is, the closer the application can simulate the user's approach. After accepting the initial parameters entered by the user, the middleware generates an initial physical topology configuration and calculates its reading rate; see the flowchart of the solution's operation presented in Figure 5. Then it starts the optimization phase by executing the simulated annealing algorithm. The steps of the optimization phase are: Generating a new physical topology configuration and calculating its reading rate; checking whether the new physical topology configuration will be accepted or not; repeating until the stop criteria are satisfied. When the optimization phase is done, the middleware displays the optimal physical topology configuration.
After that, the user can get rid of the 4 tripod systems and install the 4 UHF RFID antennas following the optimal physical topology configuration characteristics.

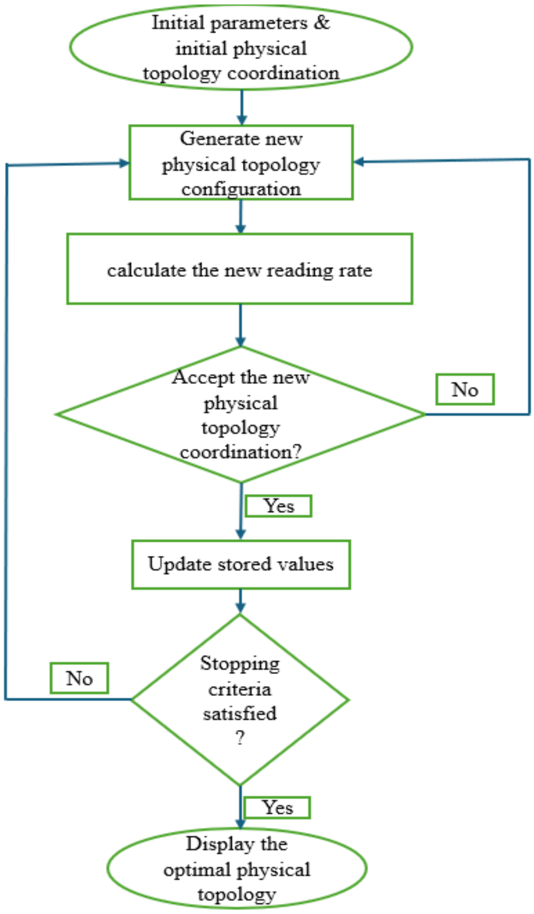

Figure 5. Solution's operation flowchart

In our middleware, each physical topology configuration is represented by an ID, four antennas (A1, A2, A3, A4), a reading rate, the temperature at which it was set; each antenna is represented by an AntiID identifier, its AiPi position and its AntRR reading rate; each antenna position is defined by its coordinates (X, Y, AntHight, AntInclination); and each RFID Tag is defined by its unique ID and the antenna that detected it.

2.3.2.2 Simulated Annealing Algorithm Design

To be able to apply the simulated annealing algorithm to find the most optimal physical topology configuration, we needed to specify the following parameters:

- The state Space is the Physical topology configuration
- The energy Function is the reading rate R.R.
- The perturbation is the changing Antennas' coordination, height, and inclination to create a new physical topology configuration
- The acceptance probability $= e^{\frac{\Delta R.R.}{T}} > rand(0,1)$. If the difference in reading rates ΔR.R.<0, the new physical topology configuration still has a chance to be accepted. This is the criterion that makes the simulated annealing algorithm able to overcome local maxima/minima to find a global maxima/minima.
- The initial Temperature = 3000 to give the algorithm the possibility to loop for a good number of iterations.
- The cooling Step = 15 so the system cools down slowly.

3. RESULTS AND DISCUSSION

3.1 Result

As we do not have a known optimal solution to compare our middleware's solution to it, we implemented two other extreme algorithms to discuss the solution quality of the simulated annealing results. The other two implemented algorithms are the Random Walk and Hill Climbing algorithms. The implementation of two different algorithms, besides the simulated annealing algorithm, and the display of their line charts are only for the analysis and evaluation of the simulated annealing results; they are not part of the solution and will be removed afterward. The line charts are presented in the figures below: Figure 6 presents the line chart of the simulated annealing algorithm, Figure 7 presents the line chart of the hill climbing algorithm, and Figure 8 presents the line chart of the random walk algorithm.

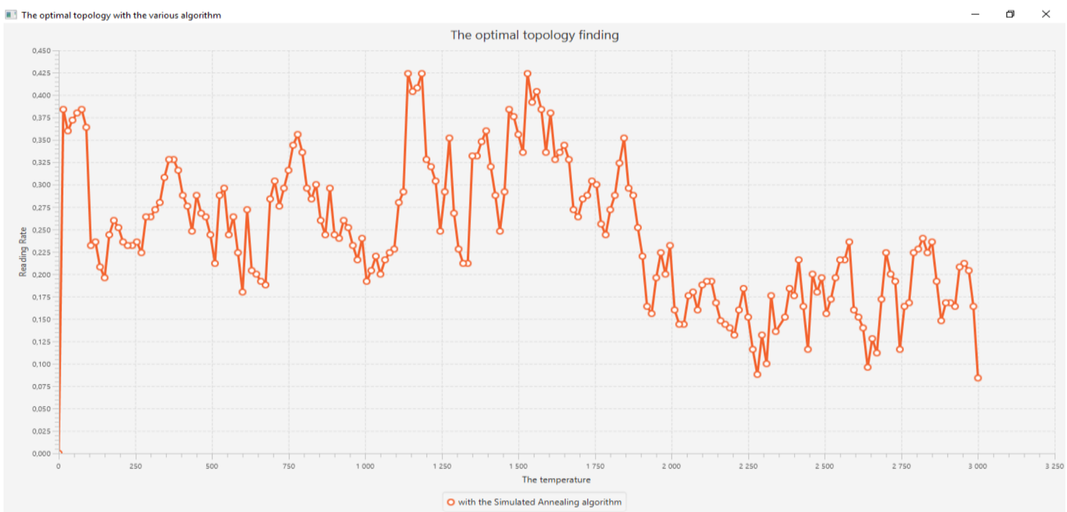

Figure 6. Simulated annealing algorithm's line chart – First run

The temperature starts to cool down from 3000 to 0 degrees with a cooling-down step equal to 15 degrees. In total, there are 200 iterations. In Figure 6, we notice that the line chart is divided into two parts: a bottom part presenting a bad quality solution and an upper part presenting a good quality solution. In the bottom part, located on the right of the line chart in Figure 6, that starts from iteration 0 to iteration 72, where temperature levels are still very high (3000 -1920), and the system still has not started to cool down yet as we have not started to reach the cooling temperature yet either, solutions' quality is bad. In fact, that down part is the system's exploration phase, where the system does not take care about solutions' quality as much as focusing more on discovering the application environment.

In the second part, located on the left of the flow chart in Figure 6, when temperature levels drop under 1905, around iteration 73, we can see that solutions start to be presented on the upper side of the diagram, which means that we started to reach better reading rates, and the flow chart start to converge toward the optimal solution. It means that around that temperature level, which is equal to 1905 in our case, we started to reach the cool-down temperature levels; the system started to cool down, finished the exploration phase, and started to focus more on finding the optimal configuration that has the best possible reading rate.

The system took 36.5% of the total iterations to discover the application environment and to start converging. Furthermore, the middleware took 48.5% of the total iterations to find the optimal physical topology configuration that has the possible maximum reading rate equal to 42.5%. So, from starting to converge, the system took 12% extra iterations to find the first optimal configuration. Moreover, to confirm that, this founded maximum reading rate that is equal to 42.5%, is actually the maximum possible, the middleware converged towards it twice again within the same run. After it took 12% extra iterations since starting to converge till it converged for the first time, it took 11.5% more iterations to converge for the second time toward that same maximum reading rate and then only 1.5% more iterations to converge for the third time toward that same maximum reading rate within the same run. Taking only 1.5% iterations to converge proves that the middleware has well explored its surrounding environment. A 42.5% reading rate is considered a good reading rate in a hostile environment with plenty of RFID constraints. During this run, we used 250 tags in total. A 42.5% reading rate means that the system detected 106 Tag in a very hostile environment where all the constraint of the passive UHF RFID technology were present. Because of its stochastic nature, it is generally unlikely for the simulated annealing (SA) algorithm to converge multiple times to the same exact optimal solution within a single run, let alone across multiple runs. The convergence behavior of SA is highly dependent on several factors, including the initial conditions, cooling schedule, degree of randomness, objective function formulation, and overall problem complexity. The results shown in Figure 6 demonstrate multiple convergences to the same optimal configuration within a single run, confirming that the selected initial conditions, randomness constraints, cooling step, and objective function were appropriately defined.

An excessively rapid cooling schedule may cause the algorithm to become trapped in a local optimum, whereas an overly slow schedule can significantly prolong the search without guaranteeing convergence. In the proposed middleware, the algorithm neither became trapped in a local maximum nor failed to converge, which validates the suitability of the chosen cooling step. During the definition of the initial parameters, we deliberately constrained the randomness of the algorithm by partitioning the reading environment into sub-environments and assigning each sub-environment to a specific antenna. Alternative strategies were considered, including allowing unrestricted antenna movement across the entire space or constraining antenna movement exclusively along diagonal paths within sub-environments. A balanced approach was ultimately adopted. The experimental results confirm the effectiveness of this design choice.

The obtained results also validate the adopted definition of the reading rate, calculated as the ratio of detected tags to the total number of tags present in the environment. This metric directly reflects identification reliability, in contrast to alternative definitions found in the literature that measure reading rate as the number of detected tags per second. The results further confirm that this formulation simplifies the problem without compromising performance assessment. Regarding the perturbation mechanism, several options were considered. One alternative involved randomly selecting both the number of antennas to be moved and their identifiers at each iteration, thereby increasing algorithmic randomness. While this approach could enhance exploration, it would also significantly increase problem complexity. To maintain simplicity and usability, we opted to perturb the current configuration by moving all antennas simultaneously—four antennas in the present implementation—at each iteration.

Since the hill-climbing algorithm is inherently greedy, it is generally susceptible to entrapment in local optima. However, comparison between the hill-climbing results (Figure 7) and the simulated annealing results (Figure 6) shows that hill climbing was able to reach the global optimum in this specific scenario. This outcome can be attributed to the relative simplicity of the test environment, the clear definition of the objective function, the straightforward computation of the reading rate, and the limited number of local optima. Nevertheless, unlike simulated annealing, hill climbing cannot identify alternative optimal configurations if the primary solution is infeasible in practice. This limitation highlights the advantage of the proposed SA-based middleware, which converges multiple times to the same optimal solution within a single run, offering both robustness and deployment flexibility.

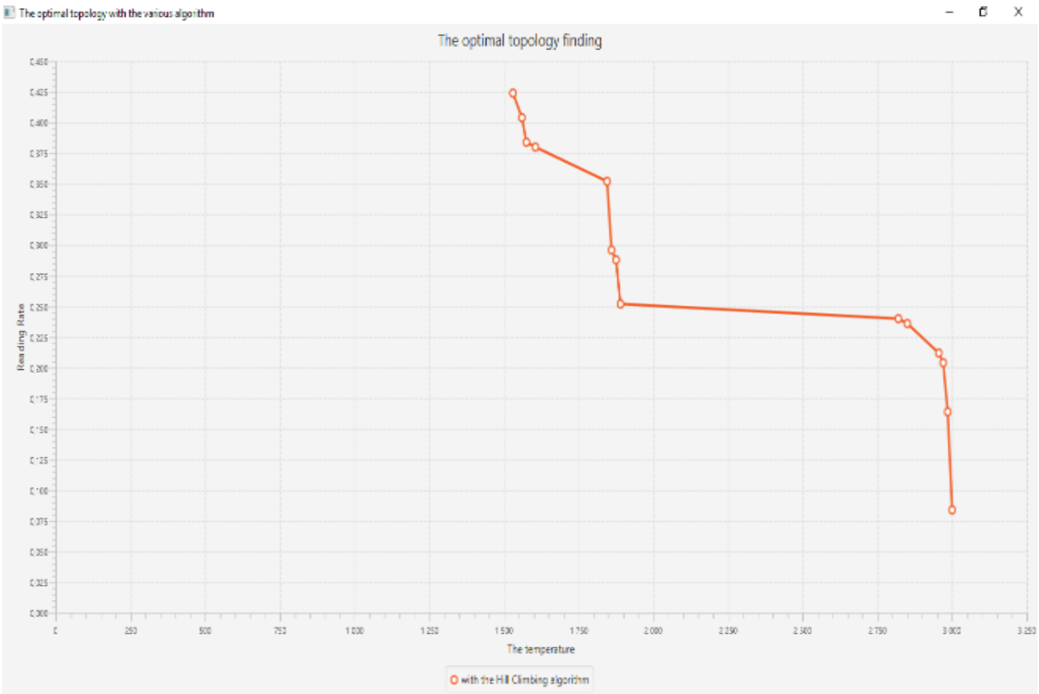

Figure. 7 Hill Climbing algorithm's line chart – first run

The Random Walk algorithm is an explorative algorithm that would accept all solutions without restriction and continue exploring the application space. By Comparing the flow chart of the Random Walk algorithm presented in Figure 8 and the line chart of the simulated annealing algorithm presented in Figure 6, we notice that also the simulated annealing algorithm has accepted all possible configurations even though his two imposed acceptance conditions: a next configuration to be accepted, her reading rate should be higher than the reading rate of the current configuration, or her acceptance probability should be higher than a random number refined between 0 and 1. Our reading rate calculation always results in a number constrained between 0 and 1, as in the worst case, if we do not detect any tags, we divide 0 by the number of used tags, which would equal 0. In the best case, if we detect all the tags used, we will divide the number of used tags by itself, and that would be equal to 1. So, this reading rate would always be less than the temperature value starting from 3000 and cooling down to 0 by a cooling step equal to 15, unless in the case where the temperature is equal to 0. So, their ratio will automatically be a number restricted between 0 and 1. This ratio presents the acceptance probability. Furthermore, the exponential of a number between 0 and 1 is a number between 1 and 2, so it will always be bigger than a random number between 0 and 1. Moreover, this is why all configurations were accepted, as their probability of acceptance, even though the temperature level is very low, reaching 15 degrees (one step before reaching 0), is always higher than a random number between 0 and 1. We conduct 3 more runs of our algorithm in 3 other different environments, and results are reported in Figure 9, Figure 10, and Figure 11.

During the second run, the most optimal reading rate is 44%, and there are 2 second most optimal reading rates equal to 42.5%. During the third run, the most optimal reading is 42.5%. During the fourth run, the most optimal reading is equal to 52%. The results of those multiple runs show the consistency of our implemented optimization algorithm through its ability to converge to an optimal solution.

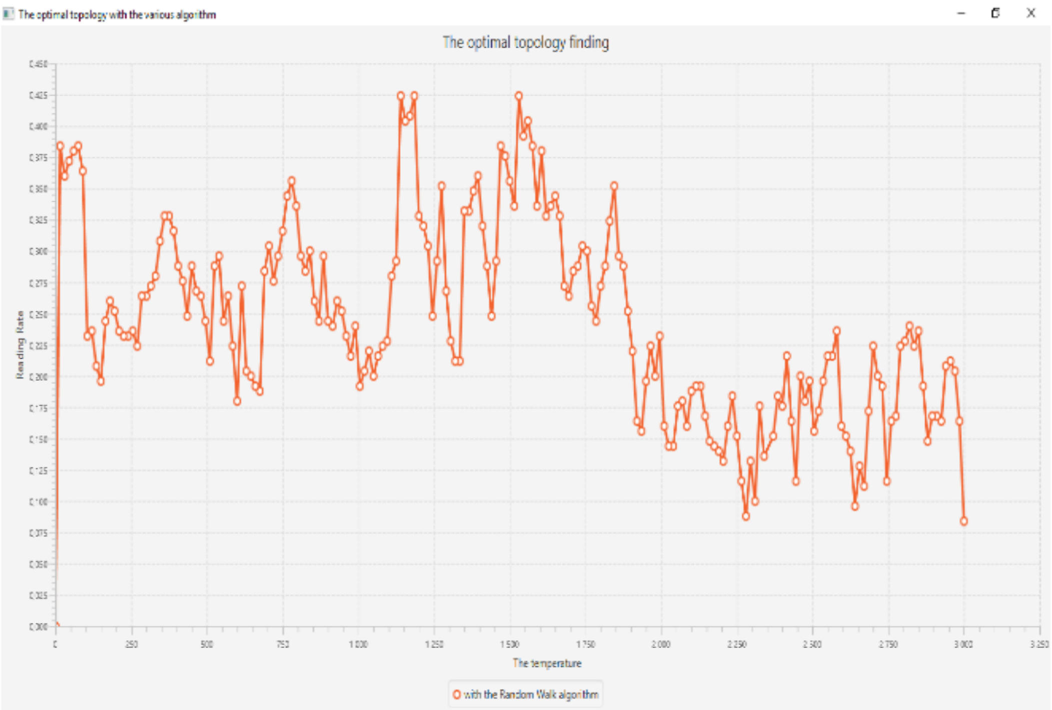

Figure. 8 Random Walk algorithm's line chart -first run

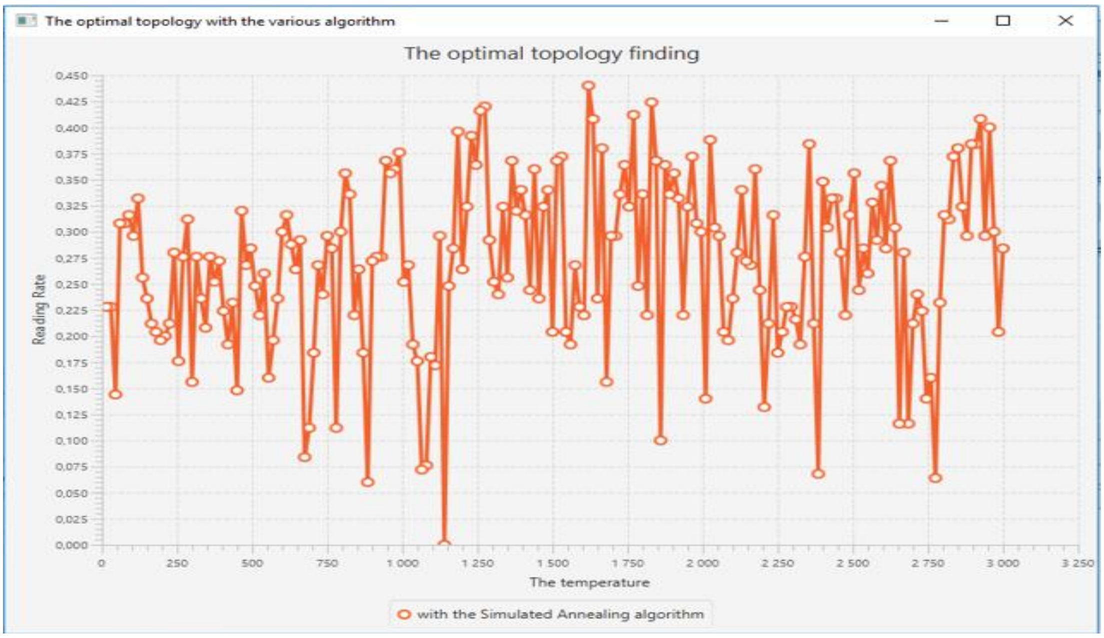

Figure 9. Simulated annealing algorithm’s line chart – second run

.

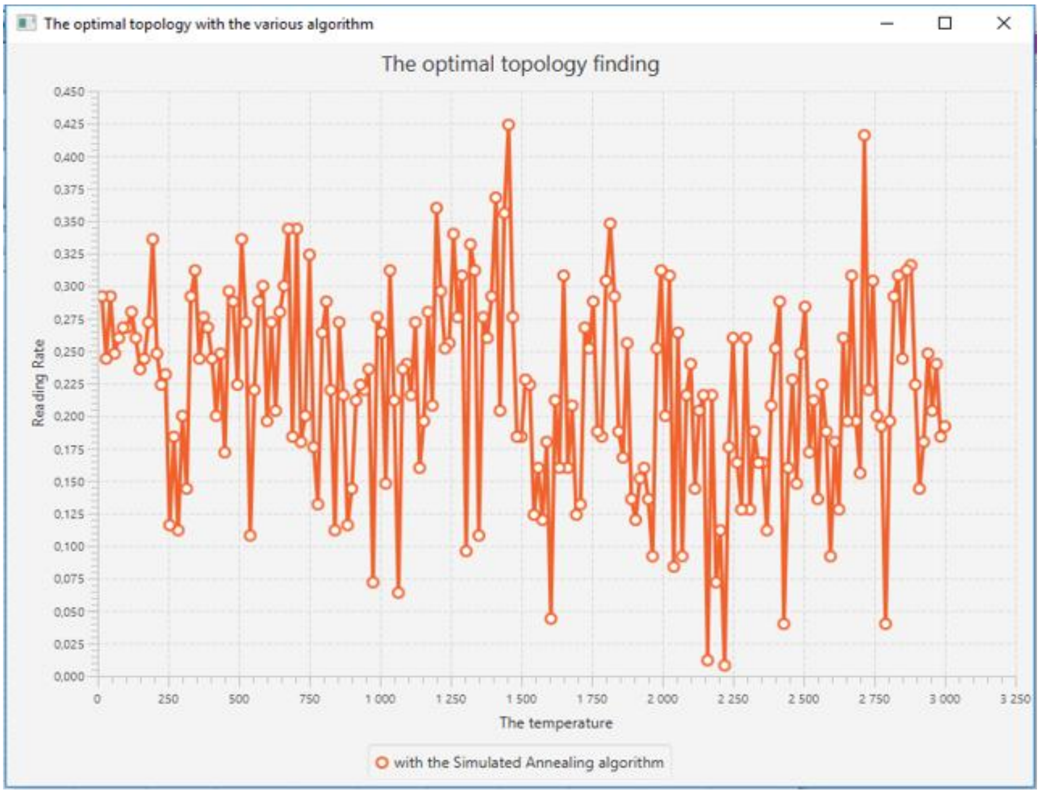

Figure 10. Simulated annealing algorithm’s line chart – Third run

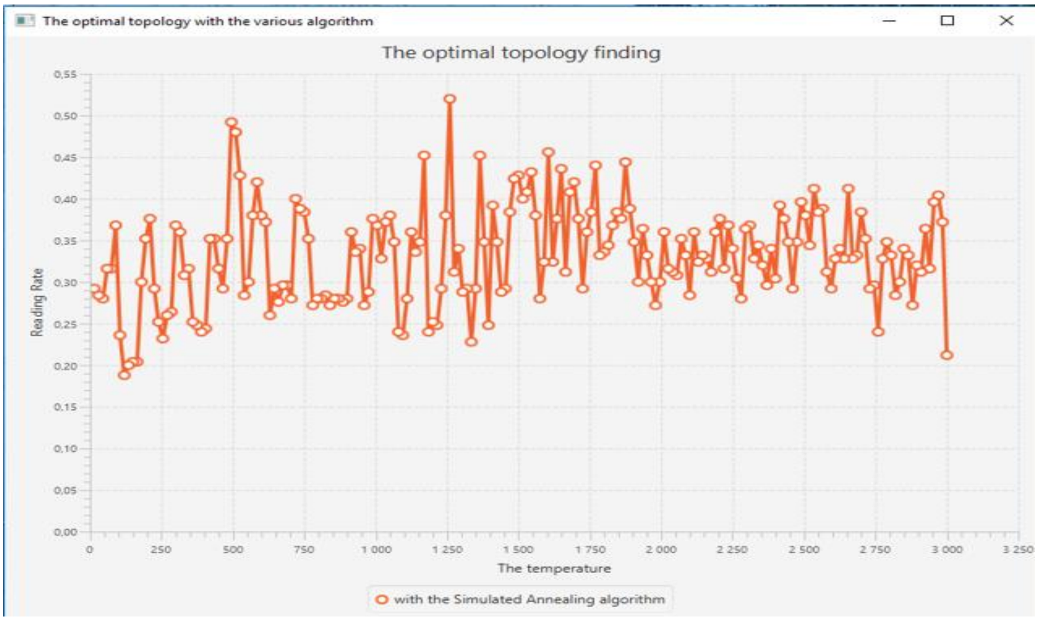

Figure 11. Simulated annealing algorithm’s line chart – Fourth run

3.2 Discussion

In this section, we will change the parameters of the optimization algorithm and discuss their influence on the results.

3.2.1 Changing the definition of the objective function

We defined the objective function of our implemented algorithm as the ratio of the number of detected tags to the number of tags to be read to estimate how many tags the system can read in such an environment. But the new definition of the objective function will be the ratio of the number of tags to be read to the read time per tag, to estimate how many tags the system can read per time unit. By comparing Figure 6 to Figure

12, we can tell this new objective function definition helped the algorithm to reject configurations without getting trapped in a local maximum.

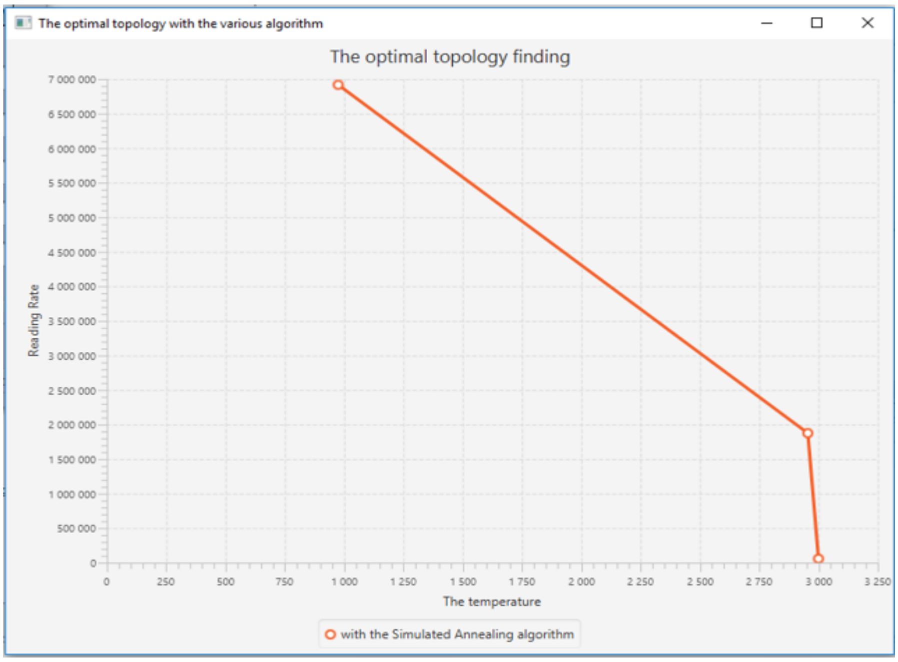

Figure 12. Simulated Annealing algorithm line chart

3.2.2 Changing algorithm randomness level and initial condition establishment

In this section, we will change the way we distribute the antennas in space. Before, the space was divided into 4 subspaces, and each antenna could be moved only within its corresponding subspace. But now, the space will not be divided, and antennas can be placed anywhere in it. The coordination, height, and inclination will still be generated randomly by the software as before. We notice from Figure 13 that the algorithm couldn't find a better configuration than the initial one.

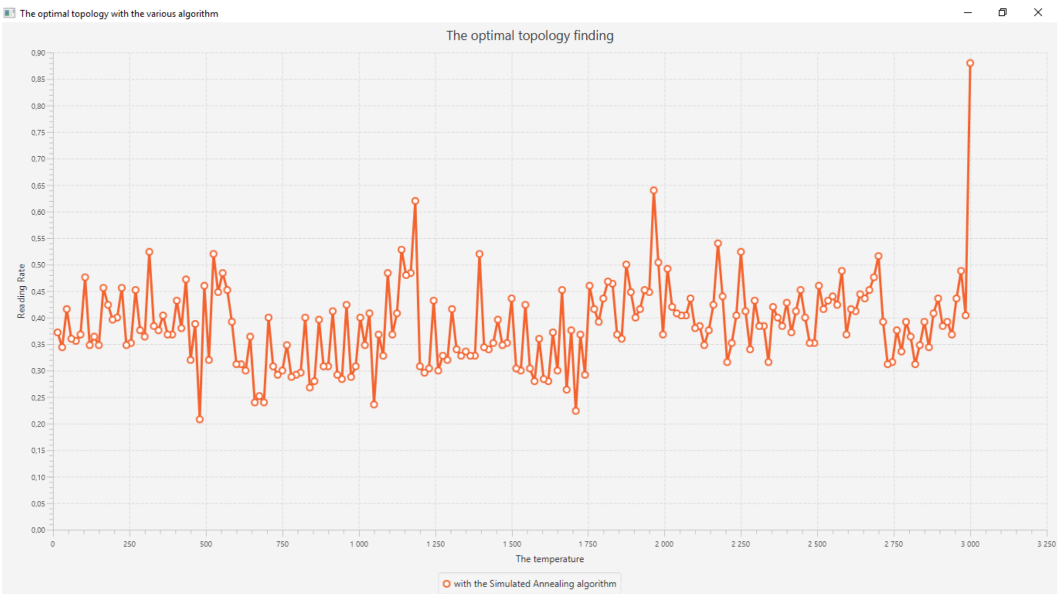

Figure 13. Simulated annealing algorithm line chart

3.2.3 Perturbation model

Before, to make a perturbation to create the next physical topology configuration, we used to change the coordination, the height, and the inclination of the 4 antennas. But now we are deciding to change the coordination of only 1 antenna. Even though the algorithm has converged, the reading rates are very low.

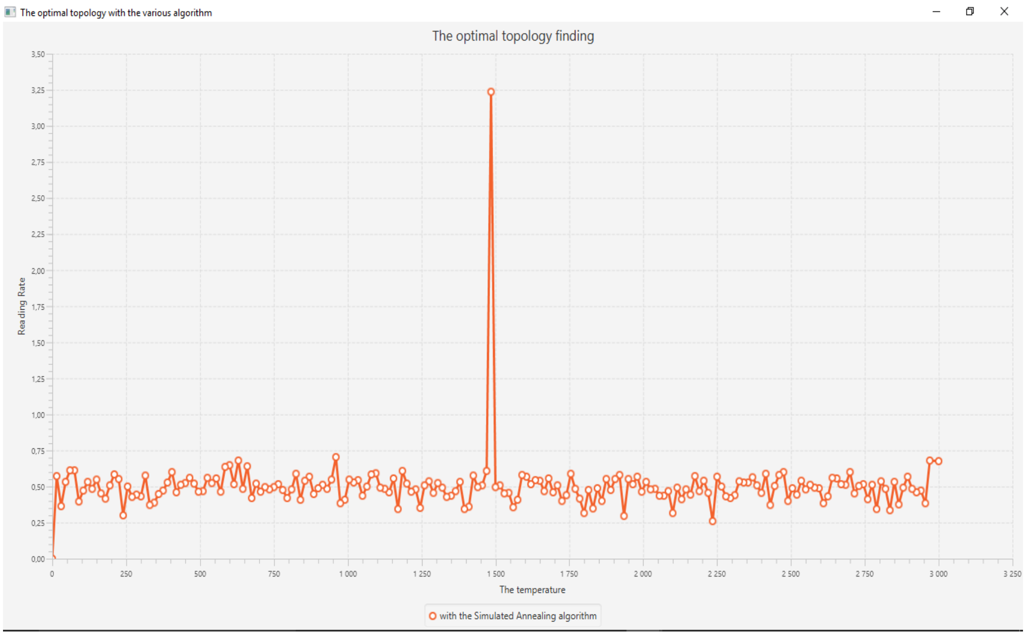

Figure 14. Simulated annealing algorithm line chart

3.2.4 Cooling Schedule

a. Initial temperature is 1000 and cooling step is 15

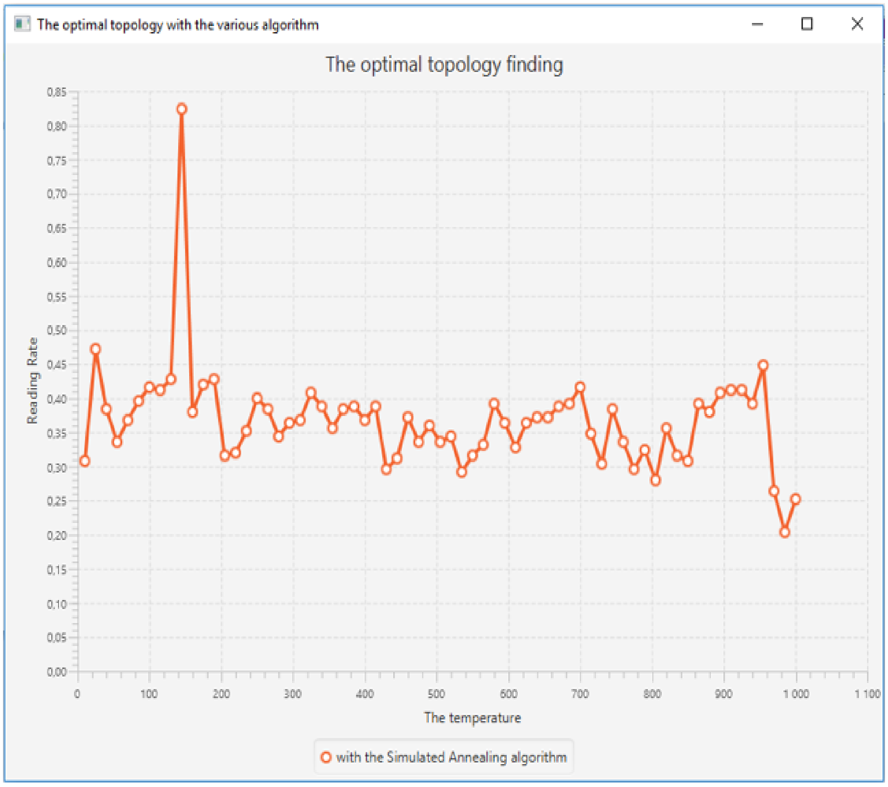

Figure 15. simulated annealing algorithm line chart

b. Initial temperature is 3000 and cooling step is 150

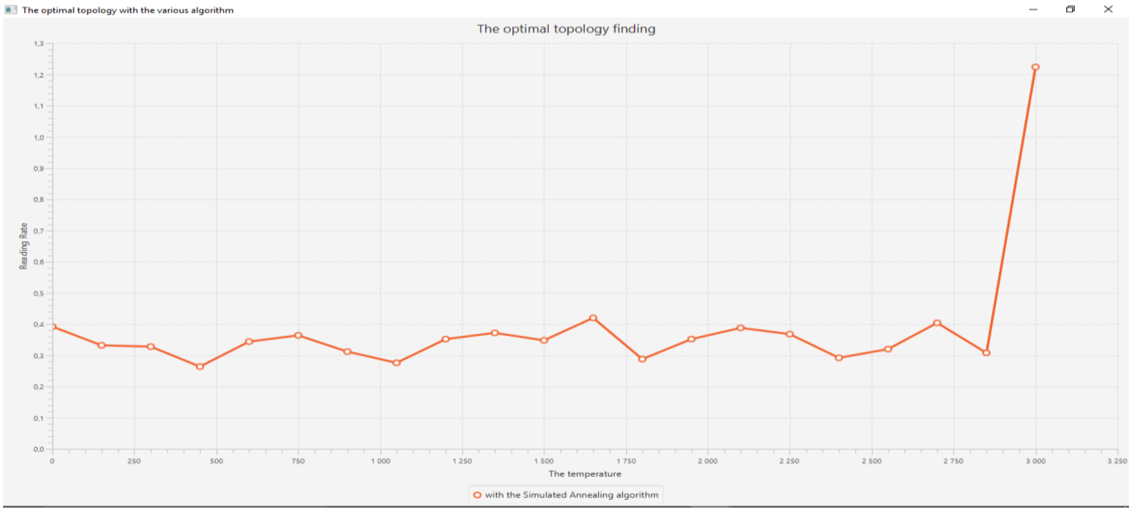

Figure 16. Simulated annealing algorithm line chart

c. Initial temperature is 1500 and cooling step is 50

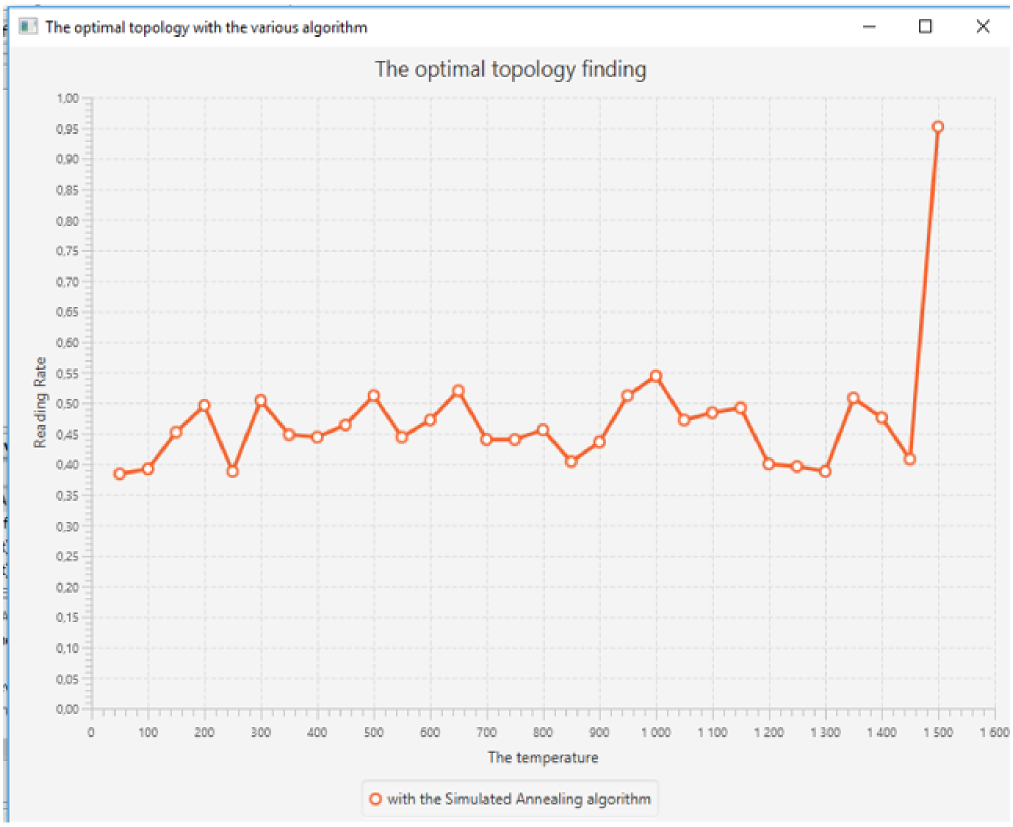

Figure 17. Simulated annealing algorithm line chart

d. Initial temperature 2000 and cooling step is 15

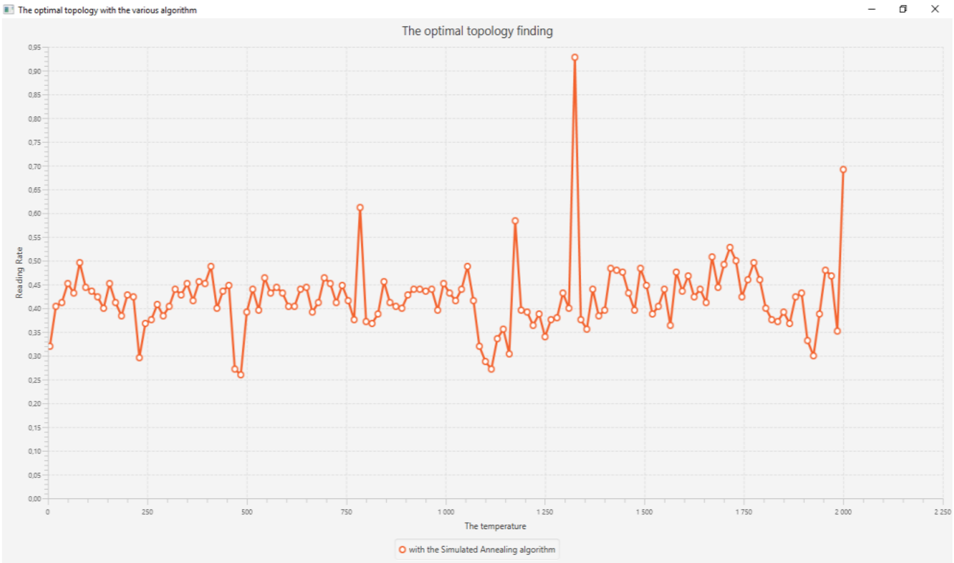

Figure 18. Simulated annealing algorithm line chart

e. Initial temperature is 6000, and the cooling step is 30

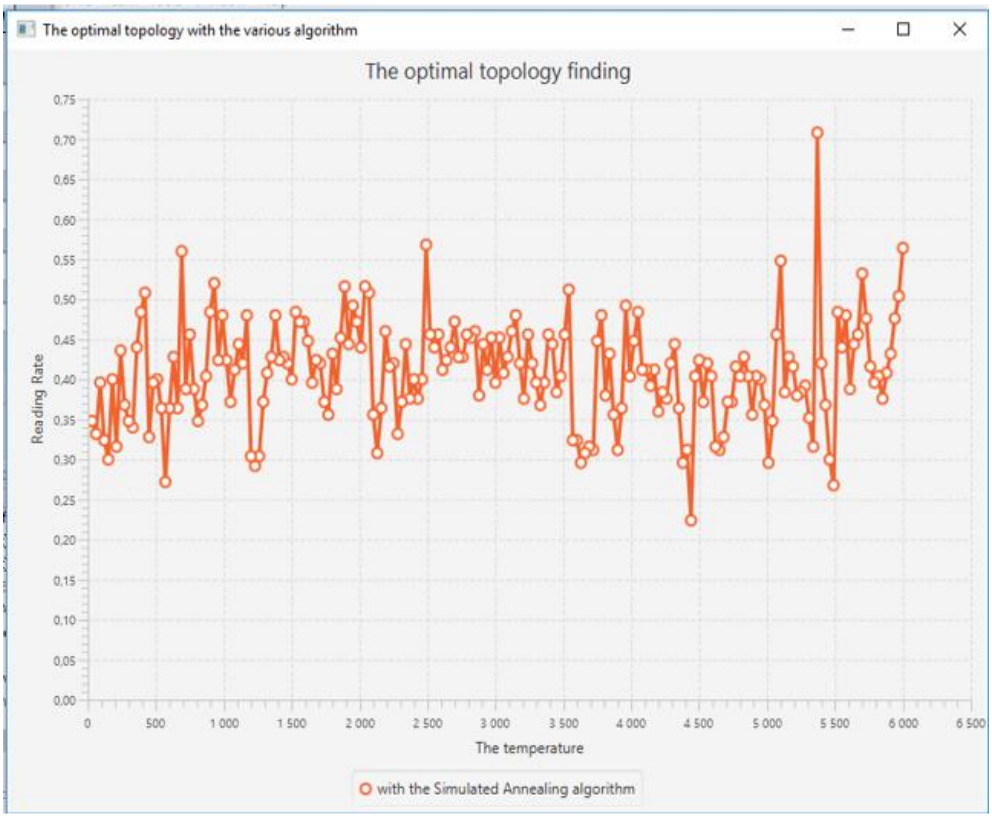

Figure 19. Simulated annealing algorithm line chart

f. Initial temperature is 1500, and the cooling step is 7

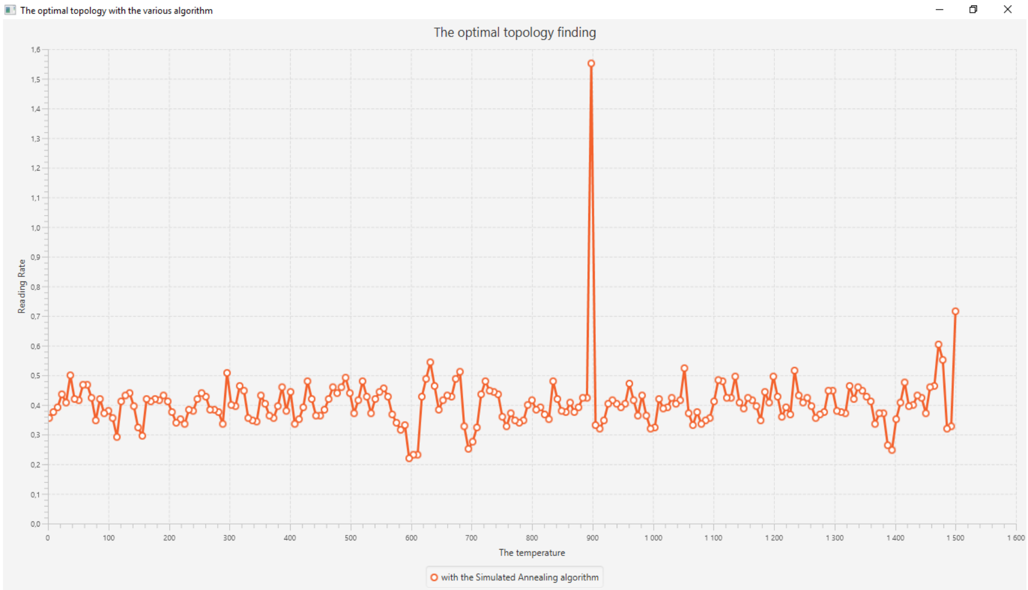

Figure 20. Simulated annealing algorithm line chart

The best cooling schedule is when the initial temperature is 2000, and the cooling step is 15.

4. CONCLUSION AND LIMITATION (10 PT)

Passive UHF RFID technology offers several compelling advantages—such as cost-effectiveness, long read range, and versatility—but remains limited by its sensitivity to environmental constraints including metals, liquids, and motion. While numerous studies have attempted to mitigate these limitations, no generalized solution has emerged. In this work, we proposed a generic passive UHF RFID identification system that adapts to diverse environments through physical topology optimization. Grounded in electromagnetic propagation theory, our approach demonstrated that improving antenna configuration can significantly enhance system performance, even under hostile conditions.

We implemented a simulated annealing algorithm to optimize the spatial layout of antennas, achieving a best reading rate of 42.5%—compared to only 7.5% in the initial configuration. The algorithm showed robustness by converging three times to the same optimal solution within a single run, requiring 48.5% of the total iterations to reach the first optimum. These results validate the effectiveness of both the optimization method and the parameter settings chosen for exploration. After multiple runs on different environments, the optimization algorithm shows good consistency. Across various RFID deployment scenarios, better results were shown when the definition of the objective function and the cooling schedule were modified.

ACKNOWLEDGEMENTS

We acknowledge the support of the Natural Sciences and Engineering Research Council of Canada.

REFERENCES

[1] H. Shall, E. Jaouadi, S. Baccar and M. Kadi, "UHF RFID Tag Antenna Performance Near Metallic Environments: A Comprehensive Characterization," *IEEE (RFID-TA)*, pp. 1-5, 2025. https://doi.org/10.1109/RFID-TA63091.2025.11265829.

[2] Y. Zhao, S. Wang and L. Zhang, "RSSI Fluctuation Analysis for RFID Tagged and Untagged Liquid Object," *International Conference on Information Science, Parallel and Distributed Systems (ISPDS)*, Guangzhou, China, pp. 662-665, 2023. https://doi.org/doi.org/10.1109/ISPDS58840.2023.10235597

[3] L. Zuo, B. Lei, L. Li, B. Li, B. Yin and L. Yuan, "Study on the Influence of Liquid Level Height in Containers on RFID System Performance," *IEEE Journal of Radio Frequency Identification*, vol. 9, pp. 758-767, 2025. https://doi.org/10.1109/JRFID.2025.3605595

[4] P. Brunet, M. Alsultan, J. Melià-Seguí and S. López-Soriano, "Experimental Analysis of UHF RFID Tags Mounted on PET Liquid Containers Subjected to External Forces", *European Conference on Antennas and Propagation (EuCAP)*, pp. 1-5, 2025. https://doi.org/10.23919/EuCAP63536.2025.10999483

[5] G. Marrocco, F. Bardati and F. Amato, “Modeling and optimization of interrogation zones in UHF RFID systems,” *IEEE Transactions on Antennas and Propagation*, vol. 57, no. 9, pp. 2575–2583, 2009. https://doi.org/10.1109/TAP.2009.2027278.

[6] M. Jankowski-Mihułowicz and M. Węglarski, “Determination of the interrogation zone in multi-antenna UHF RFID systems,” *IEEE Transactions on Microwave Theory and Techniques*, vol. 63, no. 12, pp. 4238–4249, 2015. https://doi.org/10.1109/TMTT.2015.2495185

[7] R. Jones, S. Yang, R. Penty and M. Crisp, "MU-MIMO for Passive UHF RFID," *IEEE Journal of Radio Frequency Identification*, vol. 9, pp. 215-226, 2025. https://doi.org/10.1109/JRFID.2025.3561497

[8] J. Su, H. Dong, D. Xia, A. X. Liu and B. Wang, "A Zero Trust Method for Tag Array Authentication of UHF RFID Sensing," *IEEE Transactions on Networking*. https://doi.org/10.1109/TON.2025.3599016

[9] P. C. Shen and Y. S. Chen, "Artificial Magnetic Conductor-Backed Dual-Band Circularly-Polarized RFID Reader Antenna with a Blind Spot Mitigation Metasurface," *IEEE Journal of Radio Frequency Identification*, vol. 9, pp. 320-329, 2025. https://doi.org/10.1109/JRFID.2025.3573976

[10] X. Zhang, J. Guo, Z. Lin and H. -X. Li, "Multifunctional UHF RFID Analog Sensor System Using Energy-Oriented Sequential Estimation Algorithm," *IEEE Transactions on Instrumentation and Measurement*, vol. 74, pp. 1-10, 2025, Art no. 8005810. https://doi.org/10.1109/TIM.2025.3600700

[11] S. López-Soriano, P. Brunet, M. A. Alsultan and J. Melià-Seguí, "Remote Identification of Liquids Using Absorbent Materials: A Passive UHF RFID-Based Method," *IEEE Sensors Journal*, vol. 25, no. 4, pp. 7301-7309, 2025. https://doi.org/10.1109/JSEN.2024.3524909

[12] J. Guo, Y. Zhang, X. Zhang and Z. Lin, "UHF RFID Analog Sensor System Using Power-Independent Antenna Optimization," *IEEE Antennas and Wireless Propagation Letters*, vol. 24, no. 3, pp. 651-655, 2025. https://doi.org/10.1109/LAWP.2024.3510835

[13] S. Yang, R. Jones, R. Penty and M. Crisp, "Applications in Localization and Sensing Leveraging Inter-Tag Channel Estimation," *IEEE Journal of Radio Frequency Identification*, vol. 9, pp. 874-882, 2025. https://doi.org/10.1109/JRFID.2025.3626017

[14] Y. Zhao and K. Wang, "Rewall: An RFID-based early water leak detection and localization method," *International Conference on Sensor-Cloud and Edge Computing System (SCECS)*, Zhuhai, China, 2025, pp. 387-390. https://doi.org/10.1109/SCECS65243.2025.11065517

[15] Y. Zhao, X. Liu, L. Chen, Q. Li and P. Han, "Salaft: An RFID-Based Item-Level Localization Algorithm with Fluctuation Textures," *IEEE Sensors Journal*, vol. 24, no. 6, pp. 8870-8884, 2024. https://doi.org/10.1109/JSEN.2024.3355245

[16] F. Erman, S. Koziel and L. Leifsson, "Broadband/Dual-Band Metal-Mountable UHF RFID Tag Antennas: A Systematic Review, Taxonomy Analysis, Standards of Seamless RFID System Operation, Supporting IoT Implementations, Recommendations, and Future Directions," *IEEE Internet of Things Journal*, vol. 10, no. 16, pp. 14780-14797, 2023. https://doi.org/10.1109/JIOT.2023.3289198

[17] B. Avireni, Y. Chu, E. Kepros, M. Ettorre and P. Chahal, "RFID based Vehicular Positioning System for Safe Driving Under Adverse Weather Conditions," *IEEE 73rd Electronic Components and Technology Conference (ECTC)*, Orlando, FL, USA, 2023, pp. 2196-2200. https://doi.org/10.1109/ECTC51909.2023.00380

[18] T. Porta, G. Maselli, G., C. Petrioli, "Anticollision Protocols for Single-Reader RFID Systems: Temporal Analysis and Optimization", *IEEE Transactions on Mobile Computing*, vol. 10, pp. 267-279. 2011. https://doi.org/10.1109/tmc.2010.58

[19] G. Hayytbayev, K. Küçük and M. Çavur, "A Robust Microservices Framework for Indoor Tracking System Development," *International Conference on Computer Science and Engineering (UBMK)*, 2024, pp. 1133-1137. https://doi.org/10.1109/UBMK63289.2024.10773474

[20] K. Liu, J. Yu and L. Chen, "On Information Collection in Multi-Tagged COTS RFID Systems," *IEEE Transactions on Mobile Computing*, vol. 24, no. 11, pp. 12505-12516, 2025. https://doi.org/10.1109/TMC.2025.3586660

[21] A. Lazaro, R. Villarino, M. Lazaro and D. Girbau, "Spread Spectrum Modulated mm-Wave Tag for V2X Applications," *IEEE 13th International Conference on RFID Technology and Applications (RFID-TA)*, Aveiro, Portugal, pp. 181-184, 2023. https://doi.org/10.1109/RFID-TA58140.2023.10290474

[22] B. S. Çiftler, A. Kadri and İ. Güvenc, "IoT Localization for Bistatic Passive UHF RFID Systems With 3-D Radiation Pattern," *IEEE Internet of Things Journal*, vol. 4, no. 4, pp. 905-916, 2017. https://doi.org/10.1109/JIOT.2017.2699976

[23] Z. Ali and E. Perret, "Compact Measurement Apparatus for 3D Spherical Read Range Characterization of Chipless RFID," *IEEE Access*, vol. 11, pp. 53643-53653, 2023. https://doi.org/10.1109/ACCESS.2023.3280909

[24] P. Tripicchio, S. D’Avella, M. Unetti, A. Motroni and P. Nepa, "A UHF Passive RFID Tag Position Estimation Approach Exploiting Mobile Robots: Phase-Only 3D Multilateration Particle Filters with No Unwrapping,” *IEEE Access*, vol. 12, pp. 58778-58788, 2024. https://doi.org/10.1109/ACCESS.2024.3393127

[25] L. Bianchi, E. Di Giampaolo, F. Martinelli and F. Romanelli, "Close Motion Estimation of UHF-RFID Tagged Objects Based on Electromagnetic Coupling," *IEEE Journal of Radio Frequency Identification*, vol. 8, pp. 185-195, 2024. https://doi.org/10.1109/JRFID.2024.3375795

[26] J. Wang, Y. Ma, Y. Zhao and K. Liu, "A Multipath Mitigation Localization Algorithm Based on MDS for Passive UHF RFID," *IEEE Communications Letters*, vol. 19, no. 9, pp. 1652-1655, Sept. 2015. https://doi.org/10.1109/LCOMM.2015.2450217

[27] Y. Zhang, Y. Ma, X. Miao, S. Zhang and B. Wang, "Multipath Mitigation Algorithm for Multifrequency-Based Ranging via Convex Relaxation in Passive UHF RFID," *IEEE Internet of Things Journal*, vol. 6, no. 1, pp. 744-752, 2019. https://doi.org/10.1109/JIOT.2018.2856242

[28] M. Maimouni, B. Majd, M. Bouya, "Optimising RFID network planning problem using an improved automated approach inspired by artificial neural networks", *Inf. Sci.*, 703, 121927. 2025. https://doi.org10.1016/j.ins.2025.121927
[29] A. Motroni, G. Cecchi, A. Ria and P. Nepa, "Passive UHF-RFID Technology: Integrated Communication, Localization and Sensing," *IEEE Journal of Radio Frequency Identification*, vol. 7, pp. 564-572, 2023. https://doi.org/10.1109/JRFID.2023.3301093
[30] G. Martino, M. T. Bevacqua, L. Catarinucci and M. Merenda, "Towards Multi-Frequency and Multi-View Localization via UHF-RFID Passive Tags," *IEEE International Conference on RFID Technology and Applications (RFID-TA)*, Daytona Beach, FL, USA, pp. 78-80, 2024. https://doi.org/10.1109/RFID-TA64374.2024.10965175
[31] P. Rossi, L. Catarinucci, M. Cecchini, G. Grassi and R. Colella, "Hybrid RFID-GNSS Circuit for Robust Vehicular Navigation in Signal-Degraded Environments," *IEEE Access*, vol. 13, pp. 169636-169651, 2025. https://doi.org/10.1109/ACCESS.2025.3615074
[32] P. Brunet-Gil and S. López-Soriano, "Passive Monitoring of Water Evaporation in Textile Fabrics for Industrial Applications Using a Battery-Free UHF RFID Tag," *IEEE Journal of Radio Frequency Identification*, vol. 9, pp. 682-691, 2025. https://doi.org/10.1109/JRFID.2025.3600837
[33] J. Xu et al., "The Principle, Methods and Recent Progress in RFID Positioning Techniques: A Review," *IEEE Journal of Radio Frequency Identification*, vol. 7, pp. 50-63, 2023. https://doi.org/10.1109/JRFID.2022.3233855
[34] I. N. Stancel and M. C. Surugiu, "A survey on the efficiency of the use of RFID technology in traffic management systems," *IEEE 29th International Symposium for Design and Technology in Electronic Packaging (SIITME)*, Craiova, Romania, pp. 65-72, 2023. https://doi.org/10.1109/SIITME59799.2023.10431300
[35] F. T. Zohra, O. Salim, S. Dey, H. Masoumi and N. C. Karmakar, "Machine Learning Approach to RFID Enabled Health Monitoring of Coal Mine Conveyor Belt," *IEEE Journal of Radio Frequency Identification*, vol. 7, pp. 105-117, 2023. https://doi.org/10.1109/JRFID.2023.3267361
[36] M. Xu, C. Zhao, X. Liu, X. Chen and B. Nie, "A Flexible Wireless Pressure Sensor Based on UHF RFID Technology," *IEEE Transactions on Instrumentation and Measurement*, vol. 73, pp. 1-11, 2024, Art no. 9514011. https://doi.org/10.1109/TIM.2024.3440414
[37] G. Bandini, M. Marracci, B. Tellini and A. Buffi, "ORBITER: Phase-Based Localization of RFID Tags via Circular Antenna Trajectory," *IEEE Transactions on Instrumentation and Measurement*, vol. 73, pp. 1-10, 2024, Art no. 8004110. https://doi.org/10.1109/TIM.2024.3400339
[38] T. M. Pohl, C. F. Mecklenbr√§uker and H. Arthaber, "Planar Trajectory Estimation of UHF RFIDs: Performance in Real-World Scenarios," *IEEE (RFID-TA)*, Valence, France, 2025, pp. 1-4. https://doi.org/10.1109/RFID-TA63091.2025.11265915
[39] E. Di Giampaolo, F. Martinelli and F. Romanelli, "The Role of the RFID Polarization Mismatch in the Simultaneous Localization and Mapping Problem," *IEEE Journal of Radio Frequency Identification*, vol. 7, pp. 475-485, 2023. https://doi.org/10.1109/JRFID.2023.3288373
[40] E. Di Giampaolo, F. Martinelli and F. Romanelli, "Exploiting the electromagnetic coupling to estimate the close motion of UHF-RFID tagged objects," *IEEE (RFID-TA)*, Aveiro, Portugal, pp. 201-204, 2023. https://doi.org/10.1109/RFID-TA58140.2023.10290247
[41] T. Hussain, I. Gil and R. Fernández-García, "Meander Resonator Coupled UHF RFID System for Biomechanics Sensing Applications," *IEEE Journal of Radio Frequency Identification*, vol. 9, pp. 227-235, 2025. https://doi.org/10.1109/JRFID.2025.3570441
[42] N. Barbot, O. Rance, E. Perret, "Classical RFID Versus Chipless RFID Read Range: Is Linearity a Friend or a Foe?". *IEEE Transactions on Microwave Theory and Techniques*, vol. 69, pp. 4199-4208, 2021, https://doi.org/10.1109/tmtt.2021.3077019
[43] B. Muneer, V. Palazzi, F. Alimenti, P. Mezzanotte and L. Roselli, "UHF RFID-Based Battery-Free Wireless Strain Sensor for EV Battery Management Systems," *IEEE International Conference on RFID Technology and Applications (RFID-TA)*, Valence, France, 2025, pp. 1-4. https://doi.org/10.1109/RFID-TA63091.2025.11265913
[44] C. Gocen and M. Palandoken, "UHF RFID Microwave Sensor Tag Design for an RSSI-Based Machine Learning Assisted Binary Ethanol–Water Mixture Characterization," *IEEE Sensors Journal*, vol. 24, no. 1, pp. 262-269, 2024. https://doi.org/10.1109/JSEN.2023.3332106
[45] Y. Ban et M. Kai, “Design of a UHF RFID tag antenna to keep the read range constant between on and off metal”, *IEEE International Symposium on Antennas and Propagation (APSURSI*), 2016. https://doi.org/10.1109/APS.2016.7696180
[46] R. A. Ramirez, E. A. Rojas-Nastrucci and T. M. Weller, "UHF RFID Tags for On-/Off-Metal Applications Fabricated Using Additive Manufacturing," *IEEE Antennas and Wireless Propagation Letters*, vol. 16, pp. 1635-1638, 2017. https://doi.org/10.1109/LAWP.2017.2658599
[47] S. Fu, G. Bridges and B. Kordi, "Magnetic Field Monitoring on HVdc Transmission Lines Using a UHF-RFID Tag," *2024 Photonics & Electromagnetics Research Symposium (PIERS)*, Chengdu, China, pp. 1-5, 2024. https://doi.org/10.1109/PIERS62282.2024.10618153
[48] R. B. V. B. Simorangkir et al., "Transparent Epidermal Antenna for Unobtrusive Human-Centric Internet of Things Applications," *IEEE Internet of Things Journal*, vol. 11, no. 1, pp. 1164-1174, 2024. https://doi.org/10.1109/JIOT.2023.3288994
[49] G. M. Bianco and G. Marrocco, "Joint Design of Self-Tuning UHF RFID Antenna and Microfluidic Channel for Liquid Sensing," *IEEE Journal of Radio Frequency Identification*, vol. 8, pp. 58-67, 2024. https://doi.org/10.1109/JRFID.2024.3389870

.

[50] D. Dutta, S. Genovesi, G. Manara and F. Costa, "Characterization of Material Properties by Using an Auto-Tuned RFID Chip," *4th URSI Atlantic Radio Science Meeting (AT-RASC)*, Meloneras, Spain, pp. 1-4, 2024. https://doi.org/10.46620/URSIATRASC24/KMIB8167

[51] M. T. Nguyen, Y. F. Lin, C. H. Chen, H. S. Luong and H. M. Chen, "Low Profile Planar Inverted-L Antenna (PILA) for UHF RFID Tag on Signal Absorption and Reflection Surfaces," *IEEE Access*, vol. 13, pp. 19560-19575, 2025. https://doi.org/10.1109/ACCESS.2025.3533641

[52] M. A. Alsultan, S. López-Soriano and J. Melià-Seguí, "Multitextile and Multiband UHF RFID Antenna-Based Sensor for Noninvasive eHealth Hydration Monitoring," *IEEE Sensors Journal*, vol. 25, no. 8, pp. 13974-13985, 2025. https://doi.org/10.1109/JSEN.2025.3546431

[53] S. R. Lee, W. H. Ng, E. H. Lim and S. K. A. Rahim, "Loop-Coupled Small Antenna with Enhanced Bandwidth for On-Metal UHF RFID Tag Design," *IEEE Transactions on Antennas and Propagation*, vol. 71, no. 4, pp. 3660-3664, April 2023. https://doi.org/10.1109/TAP.2023.3242079

[54] M. Murugesh, M. Firdaus Akbar and N. Azlin Ghazali, "Compact Dipolar Patch UHF RFID Tag Antenna Using Interdigital Capacitor for Metal Platforms," *IEEE Access*, vol. 13, pp. 157249-157263, 2025. https://doi.org/10.1109/ACCESS.2025.3606695

[55] M. Murugesh and M. F. Akbar, "Frequency Tunable Folded-Patch UHF RFID Tag Antenna for Metal Surfaces," in *IEEE Journal of Radio Frequency Identification*, vol. 9, pp. 976-987, 2025. https://doi.org/10.1109/JRFID.2025.3641924

[56] Y. J. Zhang, D. Wang et M. S. Tong, "An Adjustable Quarter-Wavelength Meandered Dipole Antenna with Slotted Ground for Metallically, and Airily Mounted RFID Tag", *IEEE Transactions on Antennas and Propagation*, vol. 65, no. 6, IEEE, 2017. https://doi.org/10.1109/TAP.2017.2690535

[57] C. Wu, J. Yuan and Z. Chen, "A UHF RFID Tag Antenna Placeable on a Metal Surface Without Degraded Performances," *IEEE Antennas and Wireless Propagation Letters*, vol. 23, no. 7, pp. 2101-2105, 2024. https://doi.org/10.1109/LAWP.2024.3382144

[58] T. Athauda et al., "Robust Low-Cost Passive UHF RFID Based Smart Shopping Trolley", *IEEE Journal of Radio Frequency Identification*, vol. 2, no. 3, 2018. https://doi.org/10.1109/JRFID.2018.2866087

[59] Jasmin Grosinger; Alicja Michalowska-Forsyth, "Passive Wireless Sensors in Radiation Environments", *Wireless Identification and Sensing Systems for Harsh and Severe Environments*, pp.163-201, 2025. https://doi.org/10.1002/9781394169108

[60] V. Makarovaite, A. J. R. Hillier, S. J. Holder, C. W. Gourlay and J. C. Batchelor, "Passive Wireless UHF RFID Antenna Label for Sensing Dielectric Properties of Aqueous and Organic Liquids", *IEEE Sensors Journal*, vol. 19, no. 11, pp. 4299-4307, 2019. https://doi.org/10.1109/JSEN.2019.2896481

[61] X. He, Y. Ma, T. Li, Q. Sun and Q. Feng, "Real-Time Liquid Level Monitoring with Low-Cost UHF RFID Sensors", *IEEE Sensors Journal*, vol. 25, no. 6, pp. 10261-10271, 2025. doi.org/10.1109/JSEN.2025.3528128

[62] M. A. S. Tajin, M. S. Hossain, W. M. Mongan and K. R. Dandekar, "Passive UHF RFID-Based Real-Time Intravenous Fluid Level Sensor," *IEEE Sensors Journal*, vol. 24, no. 3, pp. 3863-3873, 1 Feb.1, 2024. https://doi.org/10.1109/JSEN.2023.3342129

[63] A. Vena, S. Cahuzac, S. Dutrieux, B. Sorli and S. Naudi, "Implant-Based UHF RFID-Enabled Sensor to Detect Loosening of Knee Prosthesis," *IEEE Journal of Radio Frequency Identification*, vol. 7, pp. 536-546, 2023. https://doi.org/10.1109/JRFID.2023.3296791

[64] C. Shen, Z. Wang, J. Wu, Q. Cheng and T. Tao Ye, "Exploring RFID Technology for Wireless Control of Smart Antennas," *IEEE Internet of Things Journal*, vol. 11, no. 18, pp. 29757-29765, 2024. https://doi.org/10.1109/JIOT.2024.3407479

[65] F. -T. Zohra, O. Salim, S. Dey, H. Masoumi and N. C. Karmakar, "Machine Learning Approach to RFID Enabled Health Monitoring of Coal Mine Conveyor Belt," *IEEE Journal of Radio Frequency Identification*, vol. 7, pp. 105-117, 2023. https://doi.org/10.1109/JRFID.2023.3267361

[66] A. El-Absi, M. Maimouni and A. El-Hassani, "Multi-objective RFID reader placement optimization using evolutionary algorithms," *IEEE Access*, vol. 10, pp. 49872–49885, 2022. https://doi.org/10.1109/ACCESS.2022.3175281

[67] J. Wang, Y. Ma and K. Liu, "Adaptive calibration and parameter tuning for robust RFID localization," *IEEE Transactions on Mobile Computing,* vol. 24, no. 11, pp. 12485–12498, 2025. https://doi.org/10.1109/TMC.2025.3586642

[68] Y. Guo, H. Zhang and X. Li, "Power-independent RFID antenna optimization via topology-aware calibration," *IEEE Journal of Radio Frequency Identification*, vol. 9, pp. 510–520, 2025. https://doi.org/10.1109/JRFID.2025.3598214

[69] H. Hamam "Rethinking Intelligence: From Human Cognition to Artificial Futures", *VUBETA*, vol.2, no. 3, pp. 531-548, 2025. https://doi.org/10.26740/vubeta.v2i3.44232

[70] R. Zayoud and H. Hamam, "The Design, by Physical Topology Optimizing, of a Passive UHF RFID Identification System: Suitable for Applications with Various Constraints", *5th International Conference on Advanced Technologies for Signal and Image Processing (ATSIP)*, pp. 1-6, 2020. https://doi.org/10.1109/ATSIP49331.2020.9231580

[71] M. Periyasamy et R. Dhanasekaran, "Evaluation of performance of UHF passive RFID system in metal and liquid environment", *International Conference on Communications and Signal Processing (ICCSP)*, Melmaruvathur, India, IEEE, 2015. https://doi.org/10.1109/ICCSP.2015.7322921

[72] J. Zhang et al., "BFVP: A Probabilistic UHF RFID Tag Localization Algorithm Using Bayesian Filter and a Variable Power RFID Model", *IEEE Transactions on Industrial Electronics*, vol. 65, no. 10, pp. 8250 - 8259, 2018. https://doi.org/10.1109/TIE.2018.2803720

[73] A. Buffo et al., “A SAR-Based Measurement Method for Passive-Tag Positioning with a Flying UHF-RFID Reader”, *IEEE Transactions on Instrumentation and Measurement*, vol. 68, no. 3, pp 845 - 853, 2019. https://doi.org/10.1109/TIM.2018.2857045

BIOGRAPHIES OF AUTHORS

Habib Hamam received his B.Eng. and M.Sc. degrees in Information Processing from the Technical University of Munich, Germany, in 1988 and 1992, and his Ph.D. in Physics and Telecommunications Applications from the University of Rennes I, jointly with France Telecom Graduate School, France, in 1995. In 2004, he earned his postdoctoral diploma (Habilitation à diriger des recherches) in Signal Processing and Telecommunications from the same institution.

He held a Canada Research Chair in "Optics in Information and Communication Technologies" from 2006 to 2016 — Canada’s highest research distinction — awarded by the Government of Canada following an international peer review process. He is currently a Full Professor in the Department of Electrical Engineering at the Université de Moncton.

Professor Hamam is a Senior Member of both OSA and IEEE, a registered Professional Engineer in New Brunswick, and the recipient of multiple teaching and scientific awards. He is the founder and Editor-in-Chief of CIT-Review, Academic Editor for Applied Sciences, and Associate Editor for the IEEE Canadian Review, among others. His research interests span optical and wireless communications, diffraction, fiber components, signal and image processing, IoT, data protection, artificial intelligence, quantum technologies, and big data analytics. He can be contacted at email: habibhamam@gmail.com

Rahma ZAYOUD obtained a Master degree of Applied Science from the University of Moncton, Engineering Faculty, Canada in September 2015. She has also an engineering degree of telecommunication from a graduate school of engineering and technologies (ESPRIT) in Tunisia in 2012. Her research interests are in RFID, wireless communications, embedded systems and mobile applications. She can be contacted at email: zayoud.rahma@gmail.com

.